Mathematical Modelling and Analysis
Volume 18 Number 1, February 2013, 80–96
http://dx.doi.org/10.3846/13926292.2013.756835

Publisher: Taylor&Francis and VGTU
http://www.tandfonline.com/TMMA
Print ISSN: 1392-6292
Online ISSN: 1648-3510

Numerical Simulation of Magnetic Droplet Dynamics in a Rotating Field

Andrejs Cebers[a] **and Harijs Kalis**[a,b]

[a] *Faculty of Physics and Mathematics, University of Latvia*
Zellu ielā 8, LV-1002 Rīga, Latvia
[b] *University of Latvia*
Raina bulvāris 29, LV-1459 Rīga, Latvia
E-mail: andrejs.cebers@lu.lv
E-mail(*corresp.*): kalis@lanet.lv

Received August 27, 2012; revised November 26, 2012; published online February 1, 2013

Abstract. Dynamics and hysteresis of an elongated droplet under the action of a rotating magnetic field is considered for mathematical modelling. The shape of droplet is found by regularization of the ill-posed initial–boundary value problem for nonlinear partial differential equation (PDE). It is shown that two methods of the regularization – introduction of small viscous bending torques and construction of monotonous continuous functions are equivalent. Their connection with the regularization of the ill-posed reverse problems for the parabolic equation of heat conduction is remarked.

Spatial discretization is carried out by the finite difference scheme (FDS). Time evolution of numerical solutions is obtained using method of lines for solving a large system of ordinary differential equations (ODE).

Keywords: magnetic field, hysteresis, ill posed problem, finite differences.

AMS Subject Classification: 65M06; 65M20; 65M70; 65N06; 65F22; 65N20; 65N40.

1 Introduction

Dynamics of magnetic droplets in the rotating magnetic field is an exciting field of research. In [1] it was found that magnetic droplets with high magnetic permeability have sequence of shape bifurcations with the increase of the magnetic field including transition from oblate shape to prolate one and back to oblate at higher values of the magnetic field strength. These experimental results are in good agreement with the theoretical calculations by the virial method [1] (for more details see [4]). Later in [9, 10] it was shown that if the magnetic permeability of the droplet is enough high these bifurcations are subcritical and therefore hysteresis phenomena should occur. Behavior of the droplet at intermediate values of the rotating field strength were investigated in [7] where

further bifurcations of elongated droplets were observed, - formation of shapes with large curvature in definite places of the droplet corresponding to the discontinuities of the tangent of the center line of elongated droplet. This behavior was theoretically reproduced by the model proposed in [2], which consider the dynamics of the droplet due to the surface tension forces and torques due to the rotating magnetic field. The ill-posed nonlinear PDE for the tangent angle was derived in [2]. Its numerical solution was regularized by introducing the small viscous torques due to the bending of the droplet [13]. In our paper [3] it is shown that the regularization of the ill-posed problem may be achieved by introducing modified continuous monotonous function with discontinuous first derivative which allow us to consider the path with increasing frequencies of the rotating field. Here by applying this technique two modified functions are constructed which allow us to consider the paths with increasing and decreasing frequencies of the rotating field. As a result the existence of the multiple stationary states of the droplet in definite ranges of the frequency of rotating field and therefore hysteresis phenomena are predicted.

In the paper [5], the regularization techniques for the backward in time nonlinear parabolic problem are considered.

2 Mathematical Model

In [2] the cross section of the droplet with the length $2L$ is assumed to be circular with constant radius a. The tangential forces along the droplet are neglected. The shape of the droplet is described by the position of its centerline. The nonlinear PDE of parabolic type for the tangent angle $\beta = \beta(l,t)$ of the center line of the magnetic droplet under the action of capillary, magnetic and viscous forces is derived in the following form [2, 3]:

$$\begin{cases} \omega = \dfrac{\partial\beta}{\partial t} - \dfrac{1}{\delta}\dfrac{\partial^2}{\partial l^2}\big(\pi\gamma a\beta + M\sin(2\beta)\big) + \dfrac{3\pi a^4\eta_i}{4\delta}\dfrac{\partial^5\beta}{\partial l^4\partial t}, \\ l \in (0,2L), \quad t \in (0,t_f), \end{cases} \tag{2.1}$$

where the parameters l, η_i, t, t_f are the arc length, the intrinsic viscosity of the droplet and time with the final time moment t_f, $\beta = \omega t - \theta$ is the phase lag with angle θ between the local tangent to the centerline of the droplet and the abscissa axis (ω is the angular frequency of a rotating field), $M = \frac{2\pi^2\chi^2 H_0^2 a^2}{\mu+1}$ is the magnetic torque, $\delta = \frac{4\pi\eta}{\ln(L/a)+c}$ is the hydrodynamic drag coefficient, η_i, γ are the intrinsic viscosity and the surface tension of the droplet, χ, μ are magnetic susceptibility and permeability of magnetic liquid respectively, $H_0 = (\cos(\omega t), \sin(\omega t))$ is the rotating field, η is the viscosity of the surrounding fluid, c is a constant of the order of unity.

Shape of the droplet depending on the time in the frame of rotating field is calculated from the known tangent angle β by integration of the set of ordinary differential equations (ODEs)

$$\frac{dx}{dl} = \cos(\beta), \qquad \frac{dy}{dl} = -\sin(\beta). \tag{2.2}$$

The unknown constants of integration are determined from the condition that mass center of the droplet is motionless.

In order to present the equation (2.1) in dimensionless form, the characteristic time scale $\tau = \frac{\delta L^2}{M}$ is introduced. Arc length is scaled by L. We have following PDE:

$$\omega\tau = \frac{\partial\beta}{\partial t} - \frac{\partial^2 F(\beta)}{\partial l^2} + \epsilon\frac{\partial^5\beta}{\partial l^4\partial t}, \tag{2.3}$$

where $F(\beta) = \frac{1}{Bm}\beta + \sin(2\beta)$ is the nonlinear function, $\epsilon = \frac{3\pi a^4\eta_i}{4\delta L^4}$ is a small coefficient (of order 10^{-4}) for the regularization, $Bm = \frac{2\pi^2\chi^2 H_0^2 a^2}{(\mu+1)\gamma}$ is the magnetic Bond number given by the ratio of the magnetic and capillary forces, $l \in (0,2)$, $t \in (0,t_f)$.

The regularization term in (2.3) with parameter ϵ is added from physical considerations using the analogy between bending stress in elastic and viscous filaments [13]. The function $F(\beta)$ is not monotonic for Bm values larger than 0.5 (see Fig. 1 for $Bm = 1.5$).

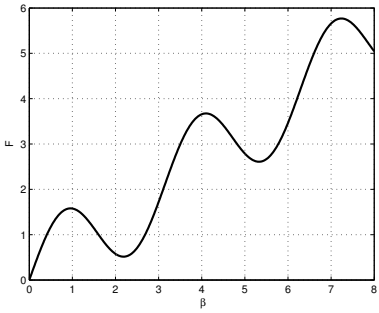

Figure 1. Function $F(\beta)$ at $Bm = 1.5$.

The equation (2.3) is supplemented by boundary conditions corresponding to the absence of normal forces and torques at the ends of the droplet: $\beta(0,t) = \beta(2,t) = \frac{\partial^2\beta(0,t)}{\partial l^2} = \frac{\partial^2\beta(2,t)}{\partial l^2} = 0$, $t \in [0,t_f)$.

The initial condition is defined by $\beta(l,0) = \Theta_0(l)$, $l \in [0,2]$, where $\Theta_0(l)$ is continuously differentiable function with $\Theta_0(0) = \Theta_0(2) = 0$. The last term in the equations (2.1), (2.3) is used for the regularization of the numerical approximations.

By setting $\epsilon = 0$ we obtain the following ill-posed problem:

$$\begin{cases} \dfrac{\partial\beta}{\partial t} = \dfrac{\partial^2 F(\beta)}{\partial l^2} + \omega\tau, \\ \beta(0,t) = \beta(2,t) = 0, \quad t \in (0,t_f), \\ \beta(l,0) = \Theta_0(l), \quad l \in [0,2]. \end{cases} \tag{2.4}$$

In the numerical experiments by changing the frequencies $\omega\tau$ we can take $\Theta_0(l)$ equal to the stationary solution obtained at the previous assigned value of the frequency.

3 Approximations and Solution of the Problems

The stationary solution $\beta_s(l)$ of the equations (2.3), (2.4) with the boundary conditions $\beta(0,t) = \beta(2,t) = 0$ can be obtained from the transcendental equation $F(\beta_s(l)) = 0.5\omega\tau l(2-l)$ for fixed values of $\omega\tau$ and $l \in (0,2)$. The maximal value $\beta_m = \beta_s(1)$ is the solution of the transcendental equation $F(\beta_m) = 0.5\omega\tau$.

The solution ($\beta(l,t) \geq 0$) is symmetrical with respect to $l = 1$: $\beta(1 - l_1, t) = \beta(1 + l_1, t)$, $l_1 \in (0,1)$ or $\frac{\partial\beta(1,t)}{\partial l} = 0$. The angle β as function of the variable l is discontinuous for $\omega\tau = 2F(\beta_0)$, where β_0 are the roots of equation $F'(\beta) = 0$ (the local maxima or minimum of the function $F(\beta)$). The values $w_c = (\omega\tau)_0 = 2F(\beta_0)$, define the critical frequencies.

The second method of regularization of the ill-posed problem (2.4) consists in construction of monotonous continuous functions. For the path with increasing frequency $\omega\tau$ of rotating field the modified (direct) function $F(\beta) = F(u)$ is constructed as follows [3]:

1) $F(u) = \frac{1}{Bm}u + \sin(2u)$, $u \in [0, u_1]$, where $u_1 = \frac{\pi}{2} - 0.5\arccos(0.5/Bm)$, is the first local maxima of function $F(u)$ or the solution of the equations $F'(u_1) = \frac{1}{Bm} + 2\cos(2u_1) = 0$,

2) $F(u) = F(u_1) = F_1$, $u \in [u_1, u_2]$, where u_2 is the solution of the transcendental equation $F(u) = F_1$ at the interval (u_1, u_3), $u_3 = \frac{3\pi}{2} - 0.5\arccos(0.5/Bm)$,

3) $F(u) = \frac{1}{Bm}u + \sin(2u)$, $u \in [u_2, u_3]$,

4) $F(u) = F(u_3) = F_3$, $u \in [u_3, u_4]$, where u_4 is the solution of the transcendental equation $F(u) = F_3$ at the interval (u_3, u_5), $u_5 = \frac{5\pi}{2} - 0.5\arccos(0.5/Bm)$,

and so on.

More generally, we can calculate the maxima of the function and the coordinates of the intersection points. Therefore in the segment $[u_{2k-1}, u_{2k}]$, $k = 1, 2, \ldots$ the function $F(u)$ is replaced with line segment $F(u) = F(u_{2k-1}) = F_{2k-1}$, where $u_{2k-1} = \frac{(2k-1)\pi}{2} - 0.5\arccos(0.5/Bm)$ are the local maxima of the function $F(u)$. The ends of the segment u_{2k-1}, u_{2k} satisfy following conditions: $u_{2k-1} = u_1 + (k-1)\pi$; $u_{2k} = u_2 + (k-1)\pi$, $k = 2, 3, \ldots$. The maximal value of $F(u_{2k-1})$ is equal $F_{2k-1} = F_1 + (k-1)\frac{\pi}{Bm}$, where $F_1 = F(u_1)$.

From $F'(u_{2k}) = F'(u_2)$, $F'(0) = 2 + \frac{1}{Bm}$ follows that $F'(u_{2k}) \leq F'(0)$. The critical frequencies $w_c(k)$ are defined by $w_c(k) = 2F_{2k-1}$, $k = 1, 2, \ldots$ This function is shown in Fig. 2 for $Bm = 1.5$.

For the path with decreasing frequency of the rotating field the modified (reverse) function $F(\beta) = f(u)$ is defined as follows:

1) $f(u) = \frac{1}{Bm}u + \sin(2u)$, $u \in [0, v_2]$, v_2 is the solution of the transcendental equation $f(u) = f_1$ at the interval $(0, u_1)$, where $f_1 = f(v_1)$ is the value of the minimal value of function $f(u)$, the local minimum is the solution of the equations $f'(u) = 0$ in the segment $[u_1, u_2]$,

2) $f(u) = f(v_1) = f_1$, $u \in [v_2, v_1]$,

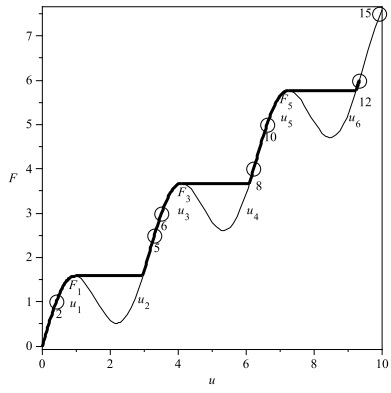

Figure 2. Direct modified function $F(u)$ at $Bm = 1.5$. The following numerical values are shown in figure: $u_1 = 0.9553$, $u_2 = 2.9448$, $u_3 = 4.0969$, $u_4 = 6.0864$, $u_5 = 7.2385$, $u_6 = 9.2280$, $F_1 = 1.5797$, $F_3 = 3.6741$, $F_5 = 5.7685$, $F'(0) = 2.6667$. In the fixed points $\odot$ there are values of $\omega\tau$ with the coordinates $(\beta_s(1), \omega\tau/2)$.

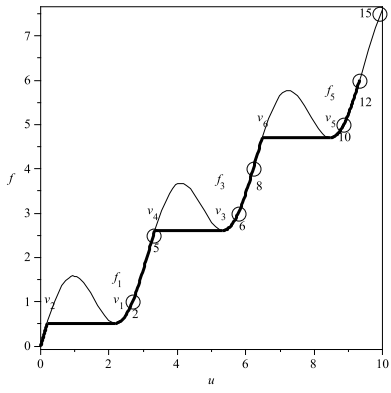

Figure 3. Reverse modified function $f(u)$ at $Bm = 1.5$. The following numerical values are shown in figure: $v_1 = 2.1863$, $v_2 = 0.1968$, $v_3 = 5.3279$, $v_4 = 3.3384$, $v_5 = 8.4695$, $v_6 = 6.4800$, $f_1 = 0.5147$, $f_3 = 2.6091$, $f_5 = 4.7035$. In the fixed points $\odot$ there are values of $\omega\tau$ with the coordinates $(\beta_s(1), \omega\tau/2)$.

3) $f(u) = \frac{1}{Bm}u + \sin(2u)$, $u \in [v_1, v_4]$, where v_4 is the solution of the transcendental equation $f(u) = f_3$ at the interval (u_2, u_3), where $f_3 = f(v_3)$ is the value of the local minimum of function $f(u)$ or the solution of the equations $f'(u) = 0$ in the segment $[u_3, u_4]$,

4) $f(u) = f(v_3) = f_3$, $u \in [v_4, v_3]$.

More generally, in the segment $[v_{2k}, v_{2k-1}]$, $k = 1, 2, \ldots$ the function $f(u)$ is replaced with line segment $f(u) = f(v_{2k-1}) = f_{2k-1}$, where $v_{2k-1} = \frac{(2k-1)\pi}{2} + 0.5 \arccos(0.5/Bm)$ are the local minimum of the function $f(u)$. The ends of the segment v_{2k-1}, v_{2k} satisfy following conditions: $v_{2k-1} = v_1 + (k-1)\pi$; $v_{2k} = v_2 + (k-1)\pi$, $k = 2, 3, \ldots$, $v_1 = \pi - u_1$. The minimal value of $f(u_{2k-1})$ is equal $f_{2k-1} = f_1 + (k-1)\frac{\pi}{Bm}$, where $f_1 = f(v_1)$. The critical frequencies $w_c(k)$ in this case are defined with the expression $w_c(k) = 2f_{2k-1}$, $k = 1, 2, \ldots$ Function $f(u)$ is shown for $Bm = 1.5$ in Fig. 3.

The stationary shapes with 3 jumps constructed according to the modified functions are shown in Fig. 4 (direct function) and Fig. 5 (reverse function) for $Bm = 1.5$, $\omega\tau = 15$. It is interesting to remark that the curvature of the shapes has opposite signs for the cases of direct and reverse functions. From $\frac{\partial^2 F(u)}{\partial l^2} = F''(u)(\frac{\partial u}{\partial l})^2 + F'(u)\frac{\partial^2 u}{\partial l^2} = -\omega\tau$ follows that $\frac{\partial^2 u}{\partial l^2} \leq 0$ if $F''(u) \geq 0$.

For the stationary solutions depending on the frequency we can obtain one or two solutions. In the segments $\omega\tau \in [2F_{2k-1}, 2f_{2k-1}]$, $k = 2, 3, \ldots$ we have two stationary solutions, but in the segments $\omega\tau \in (2F_{2k-1}, 2f_{2k+1})$, $k = 2, 3, \ldots$ the solution is unique ($F'(u) \geq 0$). An example, at $Bm = 1.5$ (see Figs. 2, 3) we have the following maximal values $\max(\beta_s(l)) = \beta_s(1)$ for different

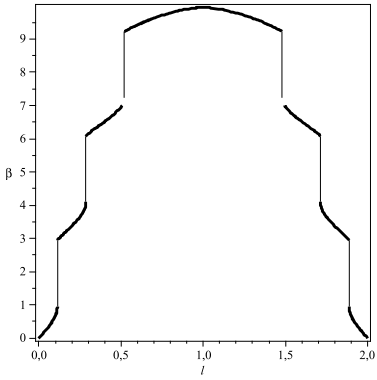

Figure 4. Stationary solution $\beta_s(l)$ at $\omega\tau = 15$ in the case of direct function.

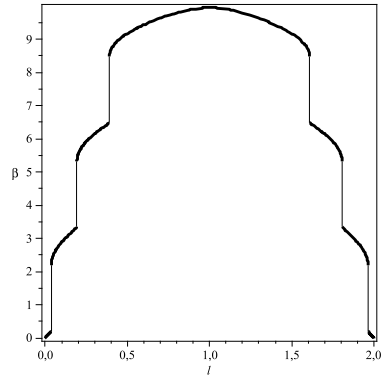

Figure 5. Stationary solution $\beta_s(l)$ at $\omega\tau = 15$ in the case of reverse function.

values of $\omega\tau$: $\omega\tau = 2(0.4078; 2.6858)$, $\omega\tau = 6(3.504, 5.7751)$, $\omega\tau = 5(3.2955)$, $\omega\tau = 8(6.2122)$, $\omega\tau = 10(6.6035, 8.8584)$, $\omega\tau = 12(9.3180)$, $\omega\tau = 15(9.9494)$.

The modified functions are continuous and monotonous with discontinuous first derivatives, $(0 \le F'(\beta) \le 2 + \frac{1}{Bm})$, and from (2.4) we can obtain that for fixed time t the solution $\beta(l,t)$ is square integrable together with the first order weak partial derivatives.

If $t = 0, \Theta_0 = 0$, then from (2.4) it follows that $\frac{\partial\beta(l,0)}{\partial t} = \omega\tau > 0$ and the function β is increasing in time. For modified functions F, f we can prove that the weak solution for fixed t is bounded in the norm of Sobolev space $\overset{0}{W}{}_2^1$ and the problem (2.4) is uniquely solvable. The solvability for the equation (2.3) with $\epsilon \neq 0$ requires an additional investigation.

The problem (2.3), which is regularized by ϵ, and problem (2.4), which is regularized by the modified functions, are solved by the MATLAB "solver ode15s" with relative error 10^{-7} (RelTol = 10^{-7}), using the method of lines and finite difference method for the approximation of spatial derivatives. We consider the uniform grid in the space $l_j = jh$, $j = \overline{0, N}$, $Nh = 2$. The finite differences of second order approximation for partial derivatives of second and fourth order with respect to l are applied. As a result the initial value problem for the system of nonlinear ODEs of the first order is obtained:

$$\begin{cases} (E + \epsilon B)\dot{U}(t) + AF\big(U(t)\big) = G, \\ U(0) = U_0, \end{cases} \tag{3.1}$$

Here E is the unit matrix of $N-1$ order, A is the standard 3-diagonal matrix of $N-1$ order with the elements $\frac{1}{h^2}\{-1; 2; -1\}$ approximating the derivative $-\frac{\partial^2}{\partial l^2}$, B is the 5-diagonal matrix of $N-1$ order with the elements $\frac{1}{h^4}\{1; -4; 6; -4; 1\}$ approximating the derivative $\frac{\partial^4}{\partial l^4}$. The first and last elements of matrix B are $B(1,1) = B(N-1, N-1) = 5/h^4$, they include finite difference expressions $u_0(t) = u_N(t) = 0$, $u_{-1}(t) = -u_2(t)$, $u_{N+1} = -u_{N-1}$ used to approximate the

artificial boundary conditions

$$\frac{\partial^2\beta(0,t)}{\partial l^2} = \frac{\partial^2\beta(2,t)}{\partial l^2} = 0.$$

It is obvious that $B = A^2$.

$U(t)$, $\dot{U}(t)$, U_0, $F(U)$, G are the column-vectors of $N-1$ order with the elements $u_j(t) \approx \beta(l_j,t)$, $\dot{u}_j(t) \approx \frac{\partial\beta(l_j,t)}{\partial t}$, $u_j(0) = \Theta_0(l_j)$, $f_j \approx F(u_j(t))$, $g_j = \omega\tau$, $j = \overline{1,N-1}$.

For the difference scheme with exact spectrum (FDSES) [3] the matrix A is replaced with the matrix WDW, where $W = W^{-1}$ is the symmetrical orthogonal matrix with elements $w_{j,k}=\sqrt{\frac{2}{N}}\sin\frac{\pi jk}{N}$, $j,k = \overline{1,N-1}$ and the diagonal matrix D contains the $N-1$ and eigenvalues $\lambda_k = (\frac{k\pi}{L})^2$ of the differential operator $(-\frac{\partial^2}{\partial l^2})$. For FDS the diagonal matrix D has eigenvalues $\mu_k = \frac{4}{h^2}\sin^2(\frac{\pi k}{2N})$.

Using the matrix form $A + \frac{h^2}{12}B$ for the fourth order approximation of the diffusion operator [12], we can obtain the following problem:

$$\begin{cases} (E+\epsilon B)\dot{U}(t) + \left(A + \dfrac{h^2}{12}B\right)F\big(U(t)\big) = G, \\ U(0) = U_0, \end{cases} \tag{3.2}$$

It should be remarked that the regularization of ill-posed backward in time linear homogeneous heat transfer equation (2.3) by term $\epsilon\frac{\partial^4\beta}{\partial^4 l}$ or $\epsilon BU(t)$ for ODEs system (3.1) is considered in the book by Lattes and Lions [8].

Inverse problems for partial differential equations and their methods of regularization are considered in the book by V.Isakov [6].

By using the Lattes and Lions regularization we will consider the following two initial value problem:

$$\begin{cases} \dot{U}(t) + \left(A + \dfrac{h^2}{12}B\right)F\big(U(t)\big) + \epsilon BU(t) = G, \\ U(0) = U_0 \end{cases} \tag{3.3}$$

and

$$\begin{cases} \dot{U}(t) + AF\big(U(t)\big) + \epsilon BU(t) = G, \\ U(0) = U_0. \end{cases} \tag{3.4}$$

Then we get the problem:

$$\frac{\partial u}{\partial t} = \frac{\partial}{\partial l}\left(g(u)\frac{\partial u}{\partial l}\right) - \epsilon\frac{\partial^4 u}{\partial l^4} + \omega\tau, \tag{3.5}$$

from which the following integral identity follows trivially:

$$\frac{\partial}{2\partial t}\int_0^2 u^2\,dl + \int_0^2 g(u)\Big(\frac{\partial u}{\partial l}\Big)^2\,dl + \epsilon\int_0^2\Big(\frac{\partial^2 u}{\partial l^2}\Big)^2\,dl = \omega\tau\int_0^2 u\,dl, \tag{3.6}$$

where $g(u) = \frac{2}{3} + 2\cos(2u)$, $-\frac{4}{3} \le g(u) \le \frac{8}{3}$, $g'(u) = -4\sin(2u)$.

In order to investigate the solvability of the corresponding initial-value problem in the Sobolev space $\overset{0}{W}{}_2^2$, to prove the existence of the weak solution and to obtain a priori estimations at fixed time t, we need to determine the parameter ϵ from the following inequality:

$$\int_0^2 g(u)\Big(\frac{\partial u}{\partial l}\Big)^2 dl + \epsilon \int_0^2 \Big(\frac{\partial^2 u}{\partial l^2}\Big)^2 dl \ge k_0 \int_0^2 \Big(\frac{\partial u}{\partial l}\Big)^2 dl,$$

or $\epsilon \ge \kappa = \max I(u)$, where $k_0 = const \ge 0$,

$$I(u) = \int_0^2 \big(k_0 - g(u)\big)\Big(\frac{\partial u}{\partial l}\Big)^2 dl \Big/ \int_0^2 \Big(\frac{\partial^2 u}{\partial l^2}\Big)^2 dl, \quad u \in \overset{0}{W}{}_2^2 .$$

From $\frac{dI(u+\epsilon_1\phi)}{d\epsilon_1} \to 0$, $\epsilon_1 \to 0$ (ϕ is arbitrary function $\in \overset{0}{W}{}_2^2$) the integral equation follows

$$-2\int_0^2 \frac{\partial^2 u}{\partial l^2}\frac{\partial^2 \phi}{\partial l^2}\, dl + \frac{1}{\kappa}\int_0^2 \Big(-g'(u)\Big(\frac{\partial u}{\partial l}\Big)^2\phi + 2\big(k_0 - g(u)\big)\frac{\partial u}{\partial l}\frac{\partial \phi}{\partial l}\Big)\, dl = 0,$$

or

$$\int_0^2 \Big(\frac{\partial^4 u}{\partial l^4} + \frac{1}{\kappa}\Big(-0.5g'(u)\Big(\frac{\partial u}{\partial l}\Big)^2 + \big(k_0 - g(u)\big)\frac{\partial^2 u}{\partial l^2}\Big)\Big)\phi\, dl = 0.$$

Since ϕ is arbitrary, then for fixed t the following nonlinear differential equation is obtained

$$\frac{\partial^4 u}{\partial l^4} + \frac{1}{\kappa}\Big(-0.5g'(u)\Big(\frac{\partial u}{\partial l}\Big)^2 + \big(k_0 - g(u)\big)\frac{\partial^2 u}{\partial l^2}\Big) = 0. \tag{3.7}$$

This equation is solved numerically by using Matlab solver "bvp4c", the following 5 boundary conditions are used

$$u(0,t) = u(2,t) = \frac{\partial^2 u(0,t)}{\partial l^2} = \frac{\partial^2 u(2,t)}{\partial l^2} = 0, \quad \frac{\partial u(0,t)}{\partial l} = 0.7.$$

The last condition is used to find κ for the fixed value of parameter k_0. The maximal value of $\kappa = 0.0143$ is obtained for $k_0 = 1.3$.

Then from (3.6) and using Hölder's inequality $|\int_0^2 u\, dl| \le \sqrt{2}\|u(t)\|$ we get the inequality

$$\frac{1}{2}\frac{d}{dt}\|u(t)\|^2 + k_0\|u_x(t)\|^2 \le \sqrt{2}\omega\tau\|u(t)\|.$$

Using the Friedrich inequality [11] $\|u\|^2 \le \frac{4}{\pi^2}\|u_x\|^2$ we obtain the inequality

$$\frac{d\|u(t)\|}{dt} + \frac{k_0\pi^2}{4}\|u(t)\| \le \sqrt{2}\omega\tau$$

from which it follows that

$$\|u(t)\| \le \|u(0)\|\exp\Big(-\frac{k_0\pi^2}{4}t\Big) + \sqrt{2}\omega\tau\frac{4}{k_0\pi^2}\Big(1 - \exp\Big(-\frac{k_0\pi^2}{4}t\Big)\Big).$$

If $k_0 = 0$, then $\|u(t)\| \le \|u(0)\| + \sqrt{2}\omega\tau t$.

For the stationary solutions $u_s(l)$ the estimate $\|u_s\| \le C_s$ is valid, where $C_s = \sqrt{2}\omega\tau\frac{4}{k_0\pi^2}$.

For the case of constant function g, by using the Fourier series

$$u(l,t) = \sum_{k=1}^{\infty} a_k(t) w_k(l), \quad w_k(l) = \sin\frac{k\pi l}{2}$$

we obtain

$$\frac{da_k(t)}{dt} = -g\lambda_k a_k(t) - \epsilon\lambda_k^2 a_k(t) + b_k,$$
$$b_k = \omega\tau\int_0^2 w_k(l)\,dl = \omega\tau\frac{2}{k\pi}\big(1-(-1)^k\big),$$

or

$$a_k(t) = \exp(\rho_k t)a_k(0) + \frac{b_k}{\rho_k}\big(\exp(\rho_k t) - 1\big),$$

where $\rho_k = -g\lambda_k - \epsilon(\lambda_k)^2$, $a_k(0) = \int_0^2 u(l,0)w_k(l)\,dl$. We have a bounded solution for $g = -|g| < 0$, when $\rho_k \le 0$ or $\epsilon \ge \max\frac{|g|}{\lambda_k} = \frac{|g|}{\lambda_1} = \frac{4|g|}{\pi^2}$. Using Matlab solver "bvp4c" with $g = -1$, $k_0 = 0$ we get from (3.7) that $\kappa = 0.4053 \approx \frac{4}{\pi^2}$.

For discrete equations (3.3), (3.4) in similar way we obtain, that $\epsilon \ge \frac{|g|}{\mu_1}$, $\epsilon \ge \frac{|g|(1+\mu_1 h^2/12)}{\mu_1}$.

Let us consider a backward in time problem with $\epsilon = 0$, $g = const > 0$ and initial condition $u_T(l) \in L_2(0,2)$

$$\begin{cases} \dfrac{\partial u}{\partial t} = g\dfrac{\partial^2 u}{\partial l^2}, \quad l \in (0,2),\ t \in (t_f, 0), \\ u(0,t) = u(2,t) = 0, \quad t \in (t_f,0), \quad u(l,t_f) = u_T(l), \quad l \in (0,2). \end{cases} \tag{3.8}$$

The Fourier coefficients of the solution are defined by

$$a_k(t) = \exp\big(g\lambda_k(T-t)\big)a_{Tk}, \quad a_{Tk} = \int_0^2 u_T(l)w_k(l)\,dl.$$

The coefficients $a_k(0)$ are uniquely determined from the relations $a_k(0) = \exp(g\lambda_k T)a_{Tk}$. These relations show that the solution $u(l,t)$ is exponentially unstable: if initial condition u_T is defined by the k-th mode, then for the solution

$$u(l,t) = \sum_{k=1}^{\infty} a_k(0)\exp(-g\lambda_k t)a_{Tk}w_k(l)$$

with $a_k(0) = \epsilon\exp(g\lambda_k T)$, we have $\|u(0)\| = \epsilon\exp(g\lambda_k T)$, while $\|u_T\| = \epsilon$.

In [8] the equation (3.8) is replaced by the regularized high-order equation

$$\frac{\partial u}{\partial t} = g\frac{\partial^2 u}{\partial l^2} + \epsilon\frac{\partial^4 u}{\partial l^4}.$$

Then $a_k(t) = \exp(g(\lambda_k - \epsilon\lambda_k^2)(T-t))a_{Tk}$ and the series for $u(l,t)$ is convergent in $L_2(0,2)$ for any u_T and any $t < T$. Moreover, when ϵ goes to 0, the regularized solutions are converging to the exact solution u of the initial problem (3.8) [6].

The second method for regularization of (2.4) is given by the initial value problem (3.1) with $\epsilon = 0$ but with the modified functions F, f. The shape of a droplet in the plane x, y is found by numerical integration of the equation (2.2)

$$\bar{x}(l,t) = \int_0^l \cos\bigl(\beta(\xi,t)\bigr)\,d\xi, \quad \bar{y}(l,t) = -\int_0^l \sin\bigl(\beta(\xi,t)\bigr)\,d\xi,$$

and the center of mass

$$M_x(t) = \frac{1}{2}\int_0^2 \bar{x}(l,t)\,dl, \quad M_y(t) = \frac{1}{2}\int_0^2 \bar{y}(l,t)\,dl.$$

Then $x(l,t) = \bar{x}(l,t) - M_x(t)$, $y(l,t) = \bar{y}(l,t) - M_y(t)$. Therefore, the mass center of the droplet is motionless. In the discrete case the trapezoid formula is used.

4 Numerical Results

Constructed direct and reverse functions allow us to calculate the dynamics of shapes corresponding to the path with increasing the frequency of rotating field starting from straight configuration and the reverse path starting from the deformed shape calculated by using direct function. The main numerical simulations are carried out by $N = 100$ and integrating the system of ODEs (3.1) in two ways:

$$1)\ \epsilon = 10^{-4}, \qquad 2)\ \epsilon = 0,$$

in the second case the modified functions F, f are used. The obtained results in either case are consistent with the maximal difference less than 0.1 percent.

4.1 Numerical results for different frequencies using the direct path

The dynamics of the tangent angle and the corresponding shapes formed in direct path obtained for $\Theta_0(l) = 0$ for different frequencies of rotating field by $Bm = 1.5$, $\omega\tau = 5, 8, 12, 24$ are shown in Figs. 6–13. Here the function $\beta(l,t)$ with 1, 2, 3 and 5 jumps at different time-moments t is shown (the stationary solution is obtained by $t_f = 6$). We note the formation of highly spiral -like shapes at large frequencies of the rotating field (see Figs. 11, 13).

In [3], by using the Matlab solver "ode15s" we have solved the same problem by taking $\epsilon = 0$. Now we compare more models, including different regularization techniques. The numerical results for parameters $\omega\tau = 8$, $N = 100$ and different systems of ODEs (3.1), (3.2), (3.3), (3.4) with $\epsilon = 10^{-4}$ and $\epsilon = 0$ are presented in Table 1. Here we analyze the dependence of the maximal value β_m of β and the number of time steps K at $t = t_f = 6$ on the different integration and regularization methods and values of parameter ε. The results are obtained with the Matlab solver "ode15s" (RelTol $= 10^{-7}$). For $\epsilon > 0$, we have

Table 1. β_m and K by $t = 6$ depending on method and ϵ.

Method	ϵ	K	β_m
(3.1) FDS	10^{-4}	685	6.2121
(3.2) FDS	10^{-4}	718	6.2122
(3.1) FDSES	10^{-4}	655	6.2130
(3.2) FDSES	10^{-4}	683	6.2140
(3.1) FDS*	0	8538	6.2121
(3.2) FDS*	0	9158	6.2120
(3.1) FDSES*	0	7377	6.2122
(3.2) FDSES*	0	8843	6.2118
(3.3) FDS	4×10^{-4}	3851	6.2117
(3.4) FDS	4×10^{-4}	3128	6.2091
(3.3) FDSES	4×10^{-4}	2916	6.2111
(3.4) FDSES	4×10^{-4}	2270	6.2114
(3.4) FDS	10^{-3}	1383	6.2109
(3.4) FDS*	0.3×10^{-4}	9869	6.2121

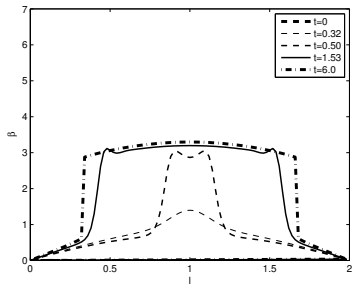

Figure 6. $\beta(l, t_i)$ with 1 jump in dependence on l for $\omega\tau = 0 \Rightarrow 5$, $t_f = 6$.

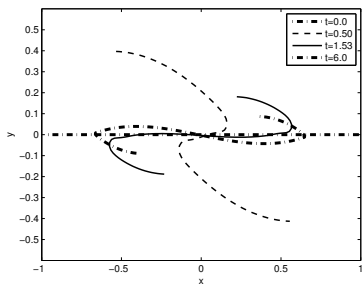

Figure 7. Droplet dynamics at $\omega\tau = 0 \Rightarrow 5$, $t_f = 6$.

observed that the computing process in time is smooth (see also Figs. 16, 17), but for $\epsilon = 0$ we have observed the oscillations in time (these cases are denoted by * in Table 1, also see Figs. 14, 15).

Remark 1. Non-stiff Matlab solvers such as "ode45" fail to converge in the ill posed case $\epsilon = 0$.

4.2 Numerical results for different frequencies using the reverse path

Relaxation of the tangent angle and the droplet shape obtained using the reverse function for $Bm = 1.5$, $\omega\tau = 5, 12, 24$ are shown in Figs. 18–25. As initial conditions for the reverse path the stationary solutions obtained for $\omega\tau$ 1 to 5, 12, 24 at $\Theta_0(l) = 0$, $t_f = 6$ are used. Figs. 20, 22 show a step-like behavior of the maximal tangent angle during the relaxation to the straight configuration which characterizes the disappearance of the jumps of tangent angle.

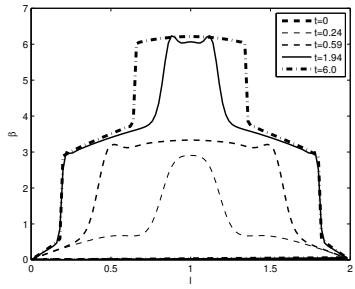

Figure 8. $\beta(l, t_i)$ with 2 jump in dependence on l for $\omega\tau = 0 \Rightarrow 8$, $t_f = 6$.

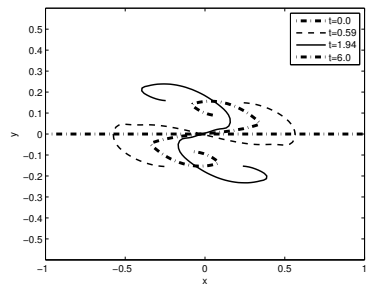

Figure 9. Droplet dynamics at $\omega\tau = 0 \Rightarrow 8$, $t_f = 6$.

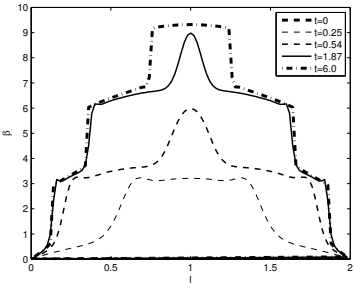

Figure 10. $\beta(l, t_i)$ with 3 jump in dependence on l for $\omega\tau = 0 \Rightarrow 12$, $t_f = 6$.

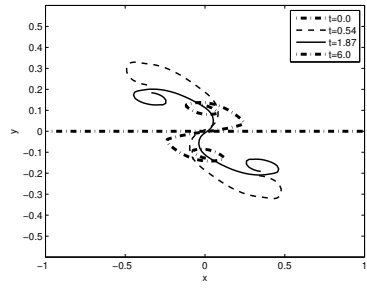

Figure 11. Droplet dynamics at $\omega\tau = 0 \Rightarrow 12$, $t_f = 6$.

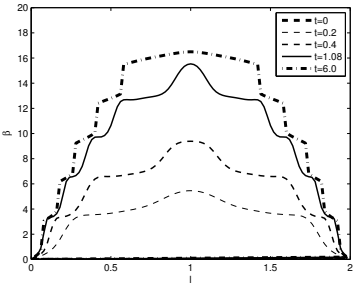

Figure 12. $\beta(l, t_i)$ with 5 jump in dependence on l for $\omega\tau = 0 \Rightarrow 24$, $t_f = 6$.

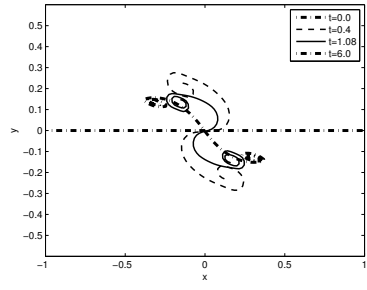

Figure 13. Droplet dynamics at $\omega\tau = 0 \Rightarrow 24$, $t_f = 6$.

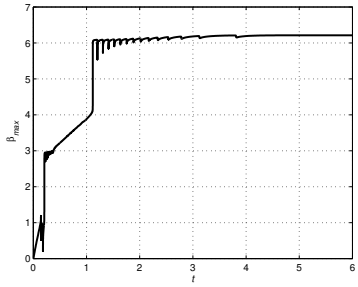

Figure 14. The dependence of $\max \beta$ on t for $\omega\tau = 0 \Rightarrow 8$, $\epsilon = 0$.

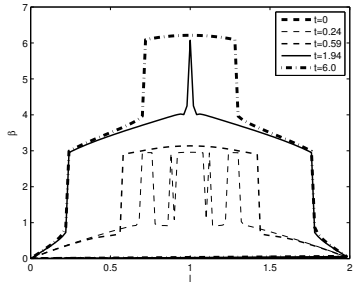

Figure 15. The dependence of $\beta(l, t_i)$ with 2 jump on l for $\omega\tau = 0 \Rightarrow 8$, $\epsilon = 0$.

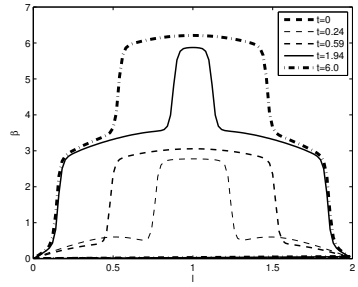

Figure 16. The dependence of $\beta(l, t_i)$ with with the Lattes and Lions regularization on l for $\omega\tau = 0 \Rightarrow 8$, $\epsilon = 4 \times 10^{-4}$.

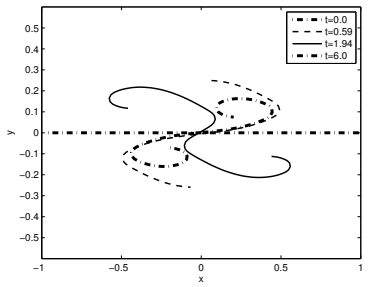

Figure 17. Droplet dynamics with the Lattes and Lions regularization at $\omega\tau = 0 \Rightarrow 8$, $\epsilon = 4 \times 10^{-4}$.

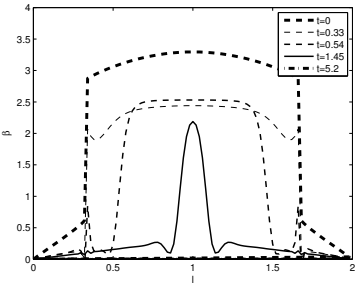

Figure 18. The dependence of $\beta(l, t_i)$ on l for $\omega\tau = 5 \Rightarrow 0$, $t_f = 6$ using reverse function.

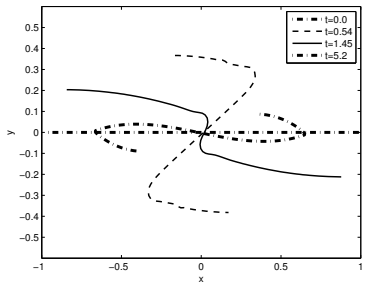

Figure 19. Droplet reverse dynamics at $\omega\tau = 5 \Rightarrow 0$, $t_f = 6$.

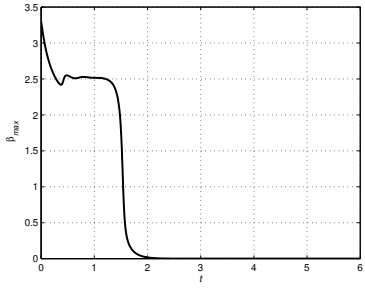

Figure 20. The dependence of $\max \beta$ on t for $\omega\tau = 5 \Rightarrow 0$ using reverse function.

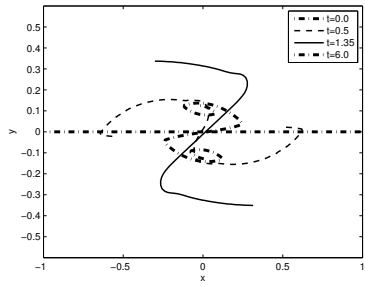

Figure 21. Droplet reverse dynamics at $\omega\tau = 12 \Rightarrow 0$, $t_f = 6$.

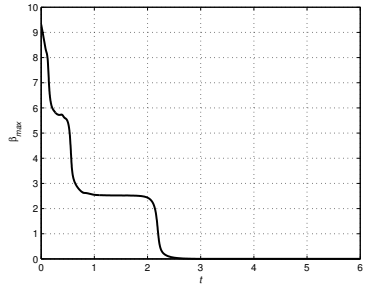

Figure 22. The dependence of $\max \beta$ on t for $\omega\tau = 12 \Rightarrow 0$ and using the reverse function.

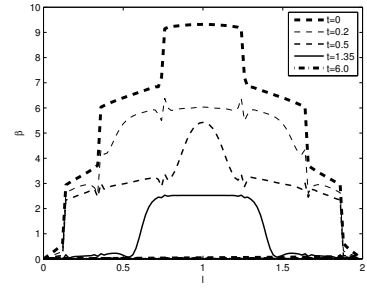

Figure 23. The dependence of $\beta(l, t_i)$ on l for $\omega\tau = 12 \Rightarrow 0$, $t_f = 6$ and using the reverse function.

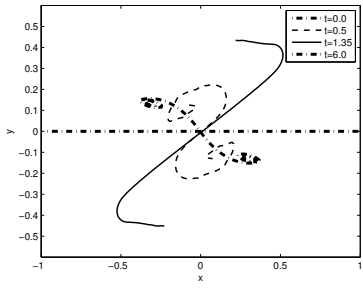

Figure 24. Droplet reverse dynamics at $\omega\tau = 24 \Rightarrow 0$, $t_f = 6$.

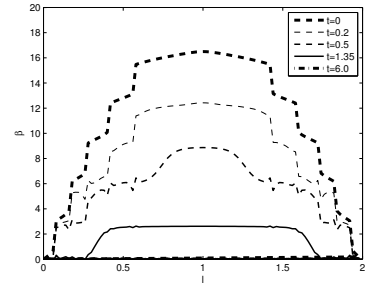

Figure 25. The dependence of $\beta(l, t_i)$ on l for $\omega\tau = 24 \Rightarrow 0$, $t_f = 6$ and using reverse function.

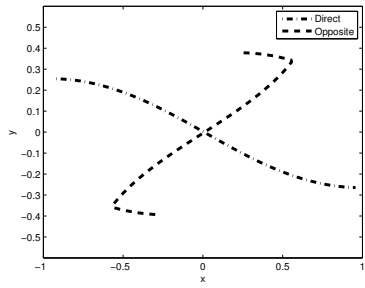

Figure 26. Droplets at $\omega\tau = 0 \Rightarrow 2 \Rightarrow 5 \cup 5 \Rightarrow 2$, $t_f = 6$.

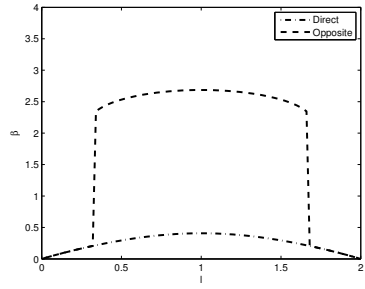

Figure 27. $\beta(l)_{stac}$ for $\omega\tau = 0 \Rightarrow 2 \Rightarrow 5 \cup 5 \Rightarrow 2$, $t_f = 6$.

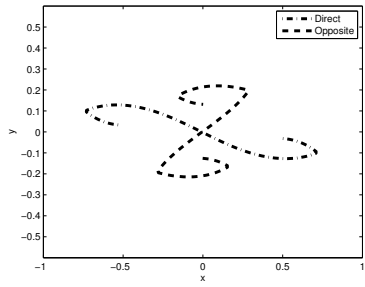

Figure 28. Droplets at $\omega\tau = 0 \Rightarrow 6 \Rightarrow 8 \cup 8 \Rightarrow 6$, $t_f = 6$.

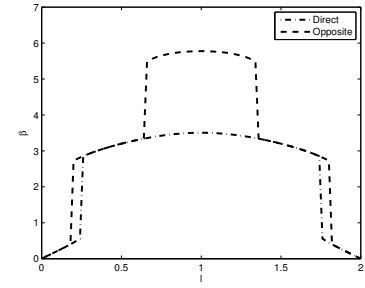

Figure 29. $\beta(l)_{stac}$ for $\omega\tau = 0 \Rightarrow 6 \Rightarrow 8 \cup 8 \Rightarrow 6$, $t_f = 6$.

4.3 Numerical results for different frequencies using the direct and reverse paths

The main results of this paper are shown in Figs. 26–31. In this case the shape obtained by reverse function starting from the stationary configuration with $t_f = 6$, which is obtained by using the direct function at higher frequency, is different from the configuration obtained at the same frequency by the direct path. So shapes obtained at $\omega\tau = 2$ by direct and reverse paths are different (see Fig. 26). Here we plot two stationary solutions at frequency $\omega\tau = 2$ obtained at $t_f = 6$ in the following way:

1) We use the direct path (function F) with $\Theta_0(l) = 0$ and obtain the stationary solutions by $\omega\tau = 2$ and $\omega\tau = 5$;

2) We use the reverse path (function f) with $\Theta_0(l)$ equal to the stationary solution obtained with the direct function for $\omega\tau = 5$ and obtain the stationary solution for $\omega\tau = 2$.

We will denote this scenario as: from 0 to 2 and to 5, then from 5 to 2 or $\omega\tau = 0 \Rightarrow 2 \Rightarrow 5 \cup 5 \Rightarrow 2$.

The same is valid for $\omega\tau = 6$, $\omega\tau = 0 \Rightarrow 6 \Rightarrow 8 \cup 8 \Rightarrow 6$ (Fig. 28) and $\omega\tau = 10$, $\omega\tau = 0 \Rightarrow 10 \Rightarrow 12 \cup 12 \Rightarrow 10$ (Fig. 30). The different tangent angle

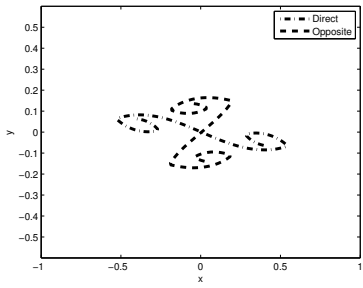

Figure 30. Droplets at $\omega\tau = 0 \Rightarrow 10 \Rightarrow 12 \cup 12 \Rightarrow 10$, $t_f = 6$.

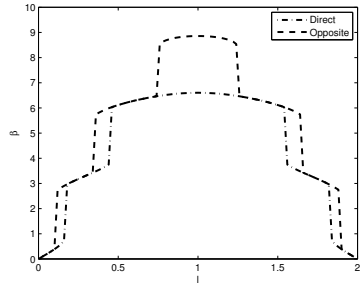

Figure 31. $\beta(l)_{stac}$ for $\omega\tau = 0 \Rightarrow 10 \Rightarrow 12 \cup 12 \Rightarrow 10$, $t_f = 6$.

for these frequencies is shown in Figs. 27, 29, 31.

Thus the considered model predicts multiple stationary states of the droplet in definite ranges of the frequency of rotating field. It would be interesting to confirm this prediction in experiments. Here we should remark that available experiments [7] indeed show the formation of the shapes with discontinuity of tangent angle which breaks at places with large curvature. The breaking phenomenon is not described by the present model.

5 Conclusions

The ill-posed problem for non-linear parabolic PDE may be regularized by introducing viscous bending torques and construction of monotonous continuous functions. By numerical simulation it is found that both approaches are equivalent. It is shown that increasing the accuracy of approximation of the discrete problem allows to decrease the number of time steps to obtain the same results.

Two monotonous functions corresponding to the paths with increasing and decreasing frequencies may be constructed and two different droplet shapes exist in definite ranges of the frequency of the rotating field. This leads to hysteresis phenomena in the droplet shape transformations at change of the frequency of rotating field. This prediction is a challenge for experimental verification.

Acknowledgement

Authors wish to thank for partial support the ESF project Nr. 2009/0223/1DP/1.1.1.2.0/09/APIA/VIAA/008 and Latvian Science Foundation grant Nr. 09.1572.

We would like to thank prof. Raimondas Čiegis from Vilnius Gediminas University for the idea of hysteresis in this problem.

References

[1] J.-C. Bacri, A. Cebers and R. Perzynski. Behavior of a magnetic fluid microdrop in a rotating magnetic field. *Phys. Rev. Lett.*, **72**:2705–2708, 1994. http://dx.doi.org/10.1103/PhysRevLett.72.2705.

[2] A. Cebers. Dynamics of an elongated magnetic droplet in a rotating field. *Phys. Rev. E*, **66**:061402, 2002. http://dx.doi.org/10.1103/PhysRevE.66.061402.

[3] A. Cebers and H. Kalis. Mathematical modelling of an elongated magnetic droplet in a rotating magnetic field. *Math. Model. Anal.*, **17**(1):47–57, 2012. http://dx.doi.org/10.3846/13926292.2012.644637.

[4] A. Cebers and S. Lacis. Magnetic fluid free surface instabilities in high-frequency rotating magnetic fields. *Brazilien J. Phys.*, **25**:101–111, 1995.

[5] R. Čiegis and A. Bugajev. Numerical approximation of one model of the bacterial self-organization. *Nonlinear Anal. Model. Control*, **17**(3):253–270, 2012.

[6] V. Isakov. *Inverse Problems for Partial Differential Equations, second edition*, volume 127 of *Appl. Math. Sci.* Springer, 2006.

[7] E. Janiaud, F. Elias, J.-C. Bacri, V. Cabuil and R. Perzynski. Spinning ferrofluid microscopic droplets. *Magnetohydrodynamics*, **36**:300–311, 2001. http://dx.doi.org/10.1023/A:1010444923379.

[8] R. Lattes and J.L. Lions. *Quasi-reversible Method and It Applications.* Mir, Moscow, 1970. (in Russian)

[9] K.I. Morozov, A. Engel and A.V. Lebedev. Shape transformations in rotating ferrofluid drops. *Europhys. Lett.*, **58**:229–235, 2002. http://dx.doi.org/10.1209/epl/i2002-00627-1.

[10] K.I. Morozov and A.V. Lebedev. Bifurcations of magnetic fluid droplet shapes in rotating magnetic field. *JETP*, **91**:1029–1033, 2000. http://dx.doi.org/10.1134/1.1334993.

[11] M. Renardy and R.C. Rogers. *An Introduction to Partial Differential Equations*, volume 13 of *Texts Appl. Math.* Springer, 1996.

[12] A.A. Samarskij. *Theory of Finite Difference Schemes.* Nauka, Moscow, 1977. (in Russian)

[13] M. Skorobogatiy and L. Mahadevan. Folding of viscous sheets and filaments. *Europhys. Lett.*, **52**:532–538, 2000. http://dx.doi.org/10.1209/epl/i2000-00470-4.